ELSEVIER

Solid State Nuclear Magnetic Resonance 11 (1998) 139–156

SOLID STATE
Nuclear Magnetic
Resonance

SQUID detected NMR and NQR

Matthew P. Augustine [a,c,*], Dinh M. TonThat [b,c], John Clarke [b,c]

[a] *Department of Chemistry, University of California, Berkeley, CA 94720, USA*
[b] *Department of Physics, University of California, Berkeley, CA 94720, USA*
[c] *Materials Sciences Division, Lawrence Berkeley National Laboratory, Berkeley, CA 94720, USA*

Abstract

The dc Superconducting QUantum Interference Device (SQUID) is a sensitive detector of magnetic flux, with a typical flux noise of the order 1 $\mu\Phi_0$ $\mathrm{Hz}^{-1/2}$ at liquid helium temperatures. Here $\Phi_0 = \hbar/2e$ is the flux quantum. In our NMR or NQR spectrometer, a niobium wire coil wrapped around the sample is coupled to a thin film superconducting coil deposited on the SQUID to form a flux transformer. With this untuned input circuit the SQUID measures the flux, rather than the rate of change of flux, and thus retains its high sensitivity down to arbitrarily low frequencies. This feature is exploited in a cw spectrometer that monitors the change in the static magnetization of a sample induced by radio frequency irradiation. Examples of this technique are the detection of NQR in ^{27}Al in sapphire and ^{11}B in boron nitride, and a level crossing technique to enhance the signal of ^{14}N in peptides. Research is now focused on a SQUID-based spectrometer for pulsed NQR and NMR, which has a bandwidth of 0–5 MHz. This spectrometer is used with spin-echo techniques to measure the NQR longitudinal and transverse relaxation times of ^{14}N in NH_4ClO_4, 63 ± 6 ms and 22 ± 2 ms, respectively. With the aid of two-frequency pulses to excite the 359 kHz and 714 kHz resonances in ruby simultaneously, it is possible to obtain a two-dimensional NQR spectrum. As a third example, the pulsed spectrometer is used to study NMR spectrum of ^{129}Xe after polariza-tion with optically pumped Rb. The NMR line can be detected at frequencies as low as 200 Hz. At fields below about 2 mT the longitudinal relaxation time saturates at about 2000 s. Two recent experiments in other laboratories have extended these pulsed NMR techniques to higher temperatures and smaller samples. In the first, images were obtained of mineral oil floating on water at room temperature. In the second, a SQUID configured as a thin film gradiometer was used to detect NMR in a 50 μm particle of ^{195}Pt at 6 mT and 4.2 K.

Keywords: dc SQUID; Optical Pumping; NMR; NQR; Spin-echo

1. Introduction

High-field Nuclear Magnetic Resonance (NMR) is an immensely powerful tool for the determination of nuclear magnetic dipole–dipole and electric quadrupole interactions in single crystal solids which, in turn, yield valuable information on inter-atomic distances and local electric field gradients [1–3]. In polycrystalline or disordered materials, however, the molecules are randomly oriented with respect to the applied magnetic field, and the resulting ‘powder pattern’ spectra may well obscure some of the structural information, particularly when the interactions are relatively weak. One solution to this problem is to remove the external magnetic field, which defines a spatial direction, and to measure the Nuclear Quadrupole Resonance (NQR) [4] or zero field NMR [5–8] directly; since all equivalent sites have the

* Corresponding author.

PII S0926-2040(97)00103-3

same resonant frequency the resulting spectra should be sharp. Examples of NQR are ^{9}Be, ^{11}B and ^{14}N in nearly symmetric environments and ^{2}D in selectively deuterated organic molecules; an example of zero field NMR is the proton resonance in polycrystalline materials.

Although this technique is an attractive approach to the acquisition of structural information in non-crystalline materials, it has the disadvantage that the corresponding resonance frequencies ω are often very low compared to those in conventional NMR and NQR: for example, the zero field NMR line in hydrated polycrystalline solids is at about 42 kHz, and the NQR line of ^{14}N in the ammonium ion is at a few tens of kilohertz. As a result, the voltage developed across a coil surrounding a collection of precessing spins is greatly reduced compared to that at tens or hundreds of megahertz. At temperature T the magnetization M scales as ω/T and the voltage as ωM, so that the induced voltage scales as ω^2/T. The small signal makes it difficult to observe low-frequency NMR or NQR with a conventional semiconductor amplifier coupled to a resonant circuit, and alternative methods have been developed. One method is magnetic field cycling [9,10], which produces the free induction decay point-by-point, and is thus rather time-consuming. An alternative way of performing zero field NMR is to spin the sample in a high magnetic field and apply radiofrequency (rf) pulses [11]. A third approach, involving a Robinson oscillator [12] in a continuous wave (cw) NQR spectrometer, has been used successfully at frequencies down to 200 kHz [13].

In this paper we describe an alternative method in which one detects the low-frequency signal directly by means of an amplifier based on a dc Superconducting QUantum Interference Device (SQUID) [14]. At kilohertz frequencies, the SQUID can have a noise temperature far below that of conventional amplifiers [14]. A unique feature of the SQUID is that it can be used to detect magnetic flux, rather than the rate of change of magnetic flux, so that at a given temperature the detected signal scales as ω rather than as ω^2. Furthermore, in this mode the input circuit is nonresonant so that one can detect signals over a broad bandwidth, from 0 to about 5 MHz. The direct detection of the spin precession induced by a pulse enables one to take advantage of the rich variety of techniques used in higher frequency NMR and NQR measurements.

We begin this paper in Section 2 with a brief overview of the dc SQUID and its operation as an amplifier. Historically, in most of the early research in this field the SQUID was used to detect NMR in cw mode in which one measures the change in static magnetic susceptibility as the radiofrequency field is swept through resonance [15–23]. In Section 3 we describe a more recent cw spectrometer and briefly discuss three recent applications in our own laboratory. The details of these experiments are kept to a minimum as they have recently been reviewed elsewhere [24]. However, as with conventional NMR, the pulsed mode is generally the more powerful technique [25–28] and in Section 4, after describing the spectrometer, we give a somewhat more detailed account of three of our recent experiments. The last two sections are concerned with experiments performed elsewhere. In Section 5 we describe an experiment in which the sample is maintained at room temperature; in particular, this spectrometer was used to obtain an image of mineral oil floating on water. Section 6 describes the use of a thin-film SQUID gradiometer to detect NMR in a tiny particle of ^{195}Pt.

2. The dc SQUID

The dc SQUID [29] combines two superconducting phenomena: flux quantization [30] and Josephson tunneling. Flux quantization demands that the net magnetic flux threading a closed superconducting loop be quantized in units of the flux quantum, $\Phi_0 = \hbar/2e = 2.07 \times 10^{-15}$ Wb, where $\hbar$ is Planck's constant and $2e$ is the charge on a Cooper pair. Thus, if we cool a ring through its superconducting transition temperature in the presence of a magnetic field and then remove the field, a persistent supercurrent flowing around the ring will maintain a flux $n\Phi_0$, where n is an integer. If we apply an external magnetic flux to the ring, the supercurrent will adjust itself to ensure that the net flux remains at $n\Phi_0$. The Josephson tunnel junction consists of two superconductors separated by a thin barrier [31,32]. Cooper pairs are able to tunnel coherently through the barrier, enabling the junction to support a supercurrent up to a maximum value known as the critical current

I_0; this zero voltage current constitutes the dc Josephson effect. When the applied current exceeds I_0, a voltage V is developed across the junction. In this regime, the supercurrents oscillate at a frequency $2\ \mathrm{eV}/\hbar = V/\Phi_0$; this is the ac Josephson effect.

The dc SQUID, shown in Fig. 1a, consists of two Josephson junctions connected in parallel on a superconducting loop of inductance L. Each tunnel junction has associated with it a capacitance C, and is shunted with an external resistance R to produce the nonhysteretic current–voltage $(I–V)$ characteristic shown in Fig. 1b. When we change the magnetic flux applied to the loop, the critical current oscillates between a maximum value at $\Phi = n\Phi_0$ and a minimum value at $\Phi = (n + 1/2)\Phi_0$; thus, the period of oscillation is Φ_0. If we bias the SQUID with an appropriate bias current I_B, the voltage correspondingly oscillates between V_1 and V_2, as indicated in Fig. 1b and c. In practice, one uses a steep portion of the $V–\Phi$ curve (Fig. 1c) to convert an oscillating flux into an oscillating voltage that can be amplified with conventional electronics. Thus, in essence, the SQUID is a flux-to-voltage transducer with a transfer coefficient $V_\Phi \equiv (\partial V/\partial \Phi)_I$. Computer simulations [33] for an optimized SQUID yield a maximum value of $V_\Phi^{\mathrm{m}} \approx R/L$; the typical values $R = 3\ \Omega$ and $L = 100$ pH yield $V_\Phi^{\mathrm{m}} \approx 60\ \mu\mathrm{V}/\Phi_0$.

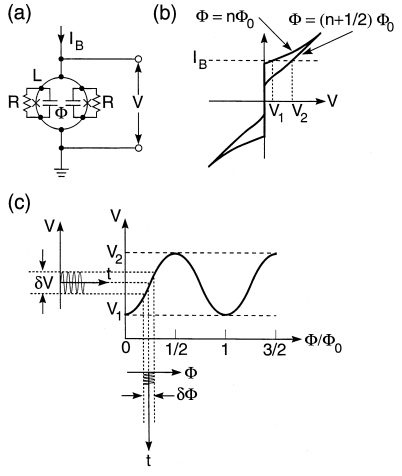

Fig. 1. (a) Configuration of dc SQUID; (b) current–voltage $(I–V)$ characteristics for an applied flux Φ of $n\Phi_0$ or $(n+1/2)\Phi_0$; (c) V vs. Φ for constant bias current I_B, indicating how flux $\delta\Phi$ is converted into voltage δV.

Modern SQUIDs are made from thin films deposited on silicon wafers and patterned photolithographically. Typically, hundreds of SQUIDs are produced on a 4-in. wafer; subsequently, the wafer is diced into chips, each with one SQUID. In the most common design [34], the body of the SQUID consists of a square washer of niobium, typically 1×1 mm^2, containing two Nb–Al_2O_3–Nb tunnel junctions. A multiturn spiral coil, also of niobium, is deposited over the square washer with an insulating layer separating the two superconducting layers. The signal current to be measured is applied to this coil; all the magnetic flux produced is forced by the superconducting washer to flow through the central hole, resulting in very efficient magnetic coupling between the coil and the SQUID.

In almost all applications, the SQUID is operated in a flux-locked loop (Section 4). A voltage induced across the SQUID by a flux change is amplified and fed, via a resistor, into a second coil also inductively coupled to the SQUID. The feedback flux opposes the applied flux, so that the SQUID is a null detector; the output voltage across the feedback resistor is proportional to the flux signal. This configuration effectively linearizes the SQUID response, enabling one to detect changes in flux ranging from a very small fraction of one flux quantum to many quanta. At frequencies f above the $1/f$ noise knee (typically 1 Hz), the spectral density $S_\Phi(f)$ of the flux noise is white; for a SQUID operating in liquid helium at 4.2 K, $S_\Phi^{1/2}(f)$ is of the order of $10^{-6}\ \Phi_0\ \mathrm{Hz}^{-1/2}$. It is useful to express this flux noise as a noise energy, $S_\Phi(f)/2L$, which is of the order of 10^{-32} J Hz^{-1} for a loop inductance $L \sim 100$ pH. It is this extraordinary energy sensitivity that enables one to measure low-frequency NQR and NMR signals with the SQUID.

To couple the flux produced by the precessing spins into the SQUID we use a superconducting flux transformer, shown schematically in Fig. 2. The pickup coil, which has an inductance L_p, is wound from Nb wire; the ends of the wire are bonded to the input coil of the SQUID, which has an inductance L_i. The closed superconducting circuit so formed must conserve magnetic flux. Thus, a flux $\delta\Phi$ coupled into the pickup coil generates a supercurrent $\delta J = -\delta\Phi/(L_i + L_p)$ in the transformer and a flux $-\delta\Phi M_i/(L_i + L_p)$ in the SQUID; here M_i is the

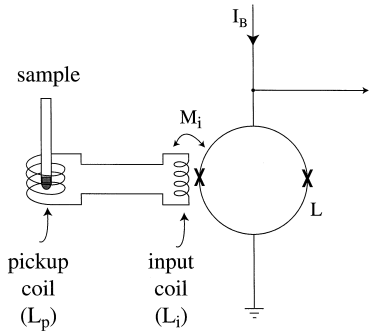

Fig. 2. Principle of flux transformer. The sample is placed in the pickup coil of inductance L_p and the input coil of inductance L_i is inductively coupled to the SQUID.

mutual inductance between the SQUID and the input coil. To a first approximation, flux transfer from the pickup loop to the SQUID is optimized when $L_i = L_p$. We note that these results hold for frequencies ranging from zero up to the frequency at which parasitic capacitance becomes significant.

We now discuss the application of the SQUID and flux transformer to cw and pulsed NMR and NQR.

3. Continuous wave spectroscopy

3.1. Introduction

In conventional cw NMR [19] the sample is placed in the coil of an LC-resonant circuit excited by an rf current. The magnetic field perpendicular to the axis of the coil is swept through resonance. At or near resonance the nuclear spins absorb power from the rf field and the precession axis swings away from the z axis, producing a voltage change across the tank circuit. In SQUID detected cw NMR or NQR [15–23,35,36], on the other hand, one detects the change in z magnetization by measuring the change in susceptibility at constant field as the excitation frequency is swept through resonance.

3.2. Spectrometer

The spectrometer for cw measurements is shown in Fig. 3 [35,36]. The NbTi pickup coil consisted of a 14-turn solenoid, 6 mm in diameter, wound on a macor form. This coil was coupled to the input terminals of a BTi dc SQUID [37], operated in a flux-locked loop. A second form surrounding the solenoid supports a Helmholtz pair of coils, orthogonal to the solenoid. A second solenoid, wound on a lead tube, could be used to supply a static magnetic field up to 3 mT before the dewar was filled with liquid ^{4}He. After the liquid had been transferred, the current in the solenoid was switched off and the field was maintained by a persistent current in the lead shield. The sample, typically 0.1 g, was packed into a Pyrex tube that could be inserted into and removed from the innermost macor tube during the course of the experiment.

A programmable frequency sweeper (Hewlett-Packard 3326A) was used to drive the Helmholtz pair at frequencies up to 13 MHz with sweep times ranging from 1 ms to 10^3 s. A major consideration in the operation of the system was the fact that the rf signal was necessarily switched on during the entire measurement. Since the solenoid could never be made completely orthogonal to the Helmholtz pair, this signal tended to interfere strongly with the operation of the SQUID. The level of interference was reduced by connecting a shunt resistor R_s across the pickup coil (Fig. 3) to make a low pass filter with a roll-off frequency that scaled with R_s. However, this resistor also injected Nyquist noise currents into the flux transformer with a spectral density that scaled

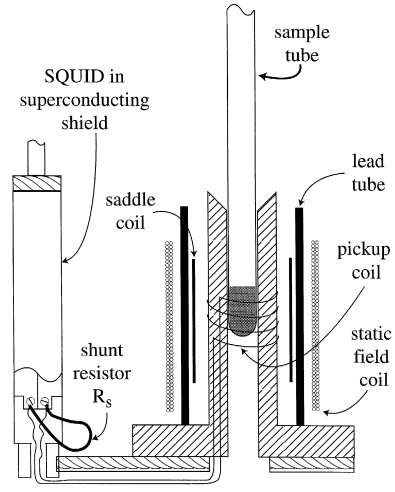

Fig. 3. Cryogenic part of cw spectrometer showing the pickup coil coupled to the SQUID, the rf saddle coil, and the copper coil and the lead tube used to produce and maintain the static field.

with $1/R_s$, reducing the signal-to-noise ratio of the measurement. As a compromise between these two conflicting requirements the resistor was chosen to give a lower limit on the rf signal of about 100 kHz. To eliminate unwanted rf interference the cryostat and the SQUID electronics were placed in a cage made of copper mesh. All the remaining electronic components were situated outside the cage.

3.3. Sapphire

Before tackling more complex problems, one needs to calibrate the system using a sample with well known properties. The ideal material will have moderately long longitudinal relaxation times, T_1, say 0.5 s to a few minutes, a large concentration of the nuclei under investigation, and a reasonable zero field splitting, say 50 kHz to 1 MHz. A sample meeting these criteria used routinely in our laboratory for calibration purposes is sapphire, α-Al_2O_3 [38]. Furthermore, high quality crystals are commercially available. Sapphire is also a good example of the use of pure NQR to determine both the quadrupolar coupling, $e^2qQ/\hbar$, and its asymmetry, η, in a single crystal sample. Since the energy of the interaction between the nuclear spin and the electric field gradients around the site of the nucleus is a function of both $e^2qQ/\hbar$ and η, knowledge of the transition frequencies between the six spin states of ^{27}Al is sufficient to determine both parameters. By measuring $e^2qQ/\hbar$ and η one can obtain information about the chemical and electronic structure surrounding the site of the nucleus [39].

The structure and quadrupole parameters for sapphire are well known. the oxygen atoms in the unit cell adopt a hexagonal close packed motif which forces an ^{27}Al nucleus to the center of an octahedron formed by six oxygen atoms [40]. In essence, an ^{27}Al nucleus is sandwiched between two equilateral triangles of oxygen atoms rotated by 60° with respect to each other. The high structural symmetry of the unit cell leads to a similar electronic symmetry implying that η should be vanishingly small. Unfortunately, one cannot use similar symmetry arguments to predict the magnitude of $e^2qQ/\hbar$; to obtain a reasonably accurate estimate of this parameter one has to perform an electronic structure calculation [39]. Since η is nearly zero in sapphire, the $+n/2>$ and $-n/2>$ states ($n = 1$, 3, or 5) are largely degenerate in energy. As a result there should be only two observable transitions, with resonance frequencies related by a factor of 2, $\upsilon_1 = \upsilon_2/2 = 3e^2qQ/20\hbar$. Indeed, as shown in Fig. 4, in zero field only two transitions with frequencies in this ratio are observed for a single crystal of sapphire. The resonance frequencies shown in Fig. 4, 357 ± 2 kHz for $|\pm 1/2> \leftrightarrow |\pm 3/2>$ and 714 ± 2 kHz for $|\pm 3/2> \leftrightarrow |\pm 5/2>$, are consistent with measurements reported at different temperatures and with different methods [41]. A detailed explanation of the observed value, $e^2qQ/\hbar = 2.389$ MHz, can be found in the literature [38,41].

Having demonstrated the operation of the cw SQUID spectrometer at low field with a NQR sapphire sample, we now move on to study more complicated and interesting chemical problems.

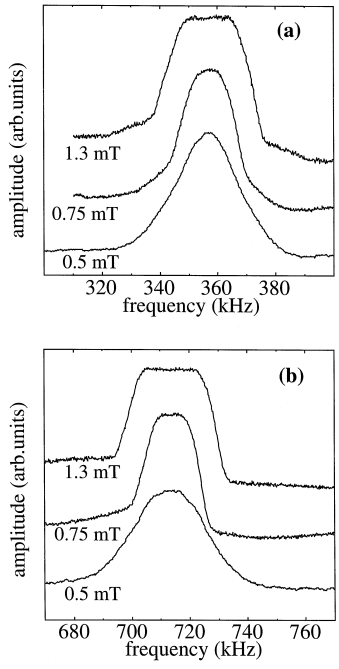

Fig. 4. NQR spectra of ^{27}Al in α-Al_2O_3 obtained in a cw spectrometer at three different applied static magnetic fields. In (a) the $|\pm 3/2> \leftrightarrow |\pm 1/2>$ resonance peak is at 357 ± 2 kHz, while in (b) the $|\pm 5/2> \leftrightarrow |\pm 3/2>$ transition occurs at 714 ± 2 kHz.

3.4. Boron nitride

Determination of the electronic structure of powdered inorganic solids is an important problem. In many cases the only characterization for these systems is electron microscopy or X-ray diffraction, techniques yielding little electronic structural information [42]. Methods such as optical spectroscopy can be used only if a transparent medium can be prepared. Solid state NMR can also be problematic because many main-group nuclei have $I > 1/2$ giving spectra that are broad and devoid of structural information. NQR, on the other hand, does not suffer from this broadening and can be a good structural probe provided that $e^2qQ/\hbar$ and η can be measured. An example of this measurement is ^{11}B in boron nitride.

The isoelectronic relation between the boron–nitrogen and carbon–carbon chemical bonds forces powdered boron nitride into a graphite like structure [43]; the boron nitride is composed of a layered network of hexagonal rings, each with three boron and three nitrogen nuclei arranged alternatively. As in the case of ^{27}Al in sapphire discussed in Section 3.3, the high symmetry leads one to expect that η will be vanishingly small. The ^{11}B NQR spectrum observed with the cw SQUID spectrometer for polycrystalline boron nitride is shown in Fig. 5 [38]. The high frequency peak at 1467 ± 2 kHz was expected from field cycling data obtained in different laboratories [44]. The inset spectrum in Fig. 5 results from a hot pressed boron nitride rod. The additional peak at 1437 ± 2 kHz is believed to be a result of the turbostratic nature of boron nitride, however, this point is not yet proven [45].

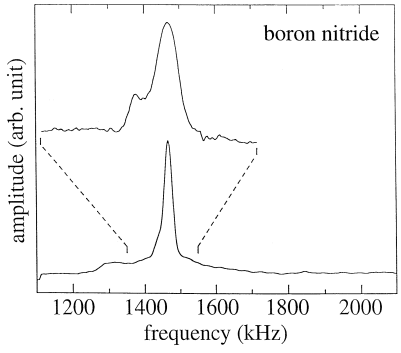

Fig. 5. ^{11}B NQR spectrum of polycrystalline boron nitride at 4.2 K in a 0.35 mT magnetic field. The peak at 1467 ± 2 kHz is assigned to the graphite-like boron nitride. The additional peak at 1437 ± 2 kHz in the inset spectrum for hot pressed boron nitride rod is still unexplained.

The relative ease of obtaining the high quality spectrum in Fig. 5 suggests that low frequency NQR in ^{11}B could be routinely studied in a wide variety of materials. For example, it would be of considerable interest to investigate boron nitride nanotubes [46] in order to clarify the electronic structure of these fullerene-like structures.

3.5. Peptides

Perhaps the most neglected nucleus in nuclear magnetic and nuclear quadrupole resonance studies is ^{14}N, which has a nuclear spin $I = 1$. It has a substantial quadrupole moment, and its high natural abundance ($\sim 99.63\%$) makes it attractive as a spectroscopic probe of structure, especially in biological systems [47]. In fact, it is this large quadrupole moment that makes high field NMR a poor technique to study ^{14}N in the liquid and solid state, since the spectra in both environments are broad and featureless. For these reasons, it was realized at an early date that the ^{14}N NQR spectrum could be used as a diagnostic tool in structural studies. For example, each amino acid has characteristic values of $e^2qQ/\hbar$ and η for the amide as well as for any side chain ^{14}N nuclei [48]. Thus, one might hope that $e^2qQ/\hbar$ and η could be used in the same way as the chemical shift in high resolution NMR to study biological structure. In particular, since one can tentatively assign an NMR spectrum for ^{1}H on the basis of the chemical shift of the functional groups, one should also be able to assign the NQR spectrum of a protein on the basis of the amino acid quadrupolar parameters.

Small splittings again plague the direct observation of the ^{14}N NQR spectrum. For this reason Slusher and Hahn combined field cycling, cross relaxation, and low temperature to obtain some of the first ^{14}N NQR spectra [49]. Although elegant, this approach is technically challenging to accomplish and a more straightforward solution involving the cw SQUID spectrometer and ^{14}N–^{1}H cross relaxation was adopted.

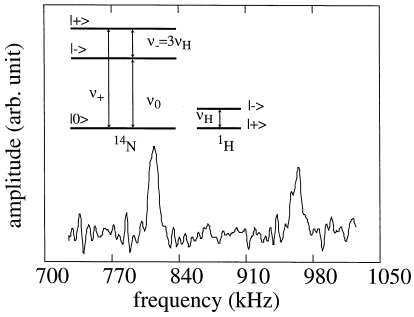

Fig. 6. ^{14}N NQR spectrum of cocaine hydrochloride showing two of the three resonances at $\nu_0 = 815$ and $\nu_+ = 965$ kHz. The inset energy level diagram shows the matching scheme where ν_- is matched to three times the ^{1}H Larmor frequency, $3\nu_H$.

In this experiment one measures the ^{1}H magnetization in a small static magnetic field while exciting the ^{14}N level populations with a perpendicular rf field. This indirect level crossing strategy offers several advantages over direct detection. Since the SQUID detects a change in the ^{1}H magnetization, the signal amplitude is increased over direct detection by the ratio of the gyromagnetic ratios of ^{1}H and ^{14}N, $\gamma_H/\gamma_N \sim 15$. Furthermore, most samples have more than one ^{1}H coupled to the ^{14}N nucleus, contributing an even larger factor to the spectral amplitude, provided ^{1}H spin diffusion is rapid. A drawback to this experiment is that one of the ^{14}N resonance frequencies must closely match a multiple of the ^{1}H Larmor frequency. Fulfilment of this condition can be both challenging and time consuming, so that, the spectrometer must remain stable for long periods of time. This limits the approach to samples with long relaxation times.

The level crossing experiment used in these studies [50] amounts to choosing a static magnetic field such that a multiple of the ^{1}H Larmor frequency is matched to one of the three possible ^{14}N transition frequencies ν_+, ν_-, or ν_0. The inset energy level diagram in Fig. 6 indicates an experiment where the ν_- transition is matched to three times the ^{1}H Larmor frequency. As the non-matched transitions are excited with the rf signal, the populations of the energy levels change. Since there is dipolar coupling between the ^{14}N and ^{1}H reservoirs, and one of the ^{14}N transitions is matched to a multiple of the ^{1}H Larmor frequency, any population change in the ^{14}N spins will be reflected in the ^{1}H magnetization [50]. As a result, the ^{14}N NQR spectrum is mapped onto a detectable variation of the ^{1}H magnetization. Table 1 summarizes the ^{14}N splittings, couplings, and asymmetries in a variety of peptides measured in this way [36], and includes references to results obtained by others using different techniques [51].

An example of a ^{14}N NQR spectrum obtained with this approach is cocaine hydrochloride, shown

Table 1
Parameters for ^{14}N in polypeptides studied with cw SQUID spectrometer [36]: resonance frequencies ν_+, ν_-, and ν_0, quadrupolar coupling constant, $C_Q = e^2qQ/\hbar$ and asymmetry parameter, η. Values for these parameters using alternative methods are given in parentheses

Peptide	Site	ν_+ (kHz)	ν_- (kHz)	ν_0 (kHz)	C_Q (kHz)	η	T (K)	Ref.
Diglycine	NH_3^+	2590 ± 3	1972 ± 3	–	3041 ± 3	0.407 ± 0.005	4.2	[36]
		(2585)	(1975)	(620)	(3030)	(0.41)	(77)	[51]
	NH	1058 ± 3	–	–	–	–	4.2	[36]
		(1090)	–	(260)	(1280)	(0.41)	(77)	[51]
Triglycine	?	1167 ± 6					4.2	[36]
	?	898 ± 8					4.2	[36]
	?	843 ± 7					4.2	[36]
	NH	(2900)		(1175)	(3080)	(0.76)	(77)	[51]
	NH	(2620)		(720)	(3010)	(0.48)	(77)	[51]
	NH_3^+	(1025)		( )	(1180)	(0.46)	(77)	[51]
L-alanyl-L-histidine	NH_3^+	1203 ± 6	933 ± 4	–	1424 ± 5	0.379 ± 0.007	4.2	[36]
	NH_3^+	1160 ± 3	834 ± 4	327 ± 5	1329 ± 4	0.491 ± 0.006	4.2	[36]
	NH	1550 ± 3	–	–	–	–	4.2	[36]
	NH	1477 ± 3	953 ± 7	524 ± 7	1620 ± 6	0.647 ± 0.008	4.2	[36]
L-alanyl-diglycine	NH_3^+	1033 ± 3	837 ± 5	183 ± 6	1247 ± 9	0.314 ± 0.014	4.2	[36]

in Fig. 6 [52]. The transitions were observed by matching the ν_- transition of ^{14}N to the triple quantum ^{1}H Larmor frequency, as shown in the inset of Fig. 6. Unfortunately this approach was not able to resolve the ν_0 transition, which is believed to occur below the lower frequency limit of the spectrometer. The results in Fig. 6 can be used to find $|e^2qQ/\hbar| = 1.186$ MHz and $\eta = 0.252$. Experiments at higher temperatures (77 K and 295 K) involving a Faraday coil detector with a sample of much larger volume confirmed these measurements.

One problem in using the cw level crossing technique to study biological structure is that in most interesting systems the ^{14}N response congests the spectrum, much as ^{1}H chemical shifts do in macromolecules. It is for this reason that current research is now focused on the pulsed SQUID spectrometer (Section 4) to develop time domain methods for measuring ^{14}N NQR spectra. It is hoped that multidimensional SQUID NQR techniques will simplify the spectra in the same way that multiple pulse NMR approaches have revolutionized structural measurements in biological systems.

4. Pulsed spectroscopy

4.1. Introduction

While the cw SQUID spectrometer is useful in many circumstances, one expects pulsed techniques to be much more powerful, for example, in obtaining time resolution and accomplishing multi-dimensional spectroscopy; one can in principle, obtain information about spin dynamics that is unavailable in cw spectroscopy. The number of systems available for study is, however, restricted because relaxation times often diverge at low temperatures, making signal averaging prohibitively long.

One uses the SQUID spectrometer in a pulsed mode to measure the free precession of the magnetization of a sample following a short pulse. In the case of NMR the magnetization precesses around a static magnetic field, and one uses a pickup coil orthogonal to both the pulse coil and the static magnetic field to couple the signal to the SQUID. For NQR spectroscopy, the precession is largely about the principal axis of the electric quadrupole tensor. In this zero magnetic field experiment the pickup coil and pulse coil are coaxial to insure that the maximum signal is delivered to the SQUID. The current SQUID spectrometer is limited to frequencies up to 5 MHz. Although one could extend this frequency range, there is little incentive to do so as conventional techniques using an LC resonant circuit become competitive above a few megahertz.

4.2. Spectrometer

The spectrometer consists of three main components: a fast flux-locked SQUID, a sample cell and a computer-controlled system for supplying the rf pulses to the sample and recording the response. We briefly describe each in turn.

The SQUIDs, made at UC Berkeley, consist of square washers of niobium with inner and outer dimensions of 40 and 900 μm and an inductance of about 100 pH. Each junction has a typical critical current of 20 μA and is shunted with a 3 Ω resistor. The 48-turn Nb spiral input coil deposited on the square washer has a mutual inductance to the SQUID of 3.5 nH and an estimated self-inductance of about 150 nH. We make superconducting contact to the coil by wire-bonding 50 μm annealed Nb wire to the Nb pads; 5 μm Nb foil is spot welded to each wire and also to a 125 μm Nb wire. The SQUID is enclosed in a hermetically sealed G-10 fiberglass tube which is surrounded by a Nb tube.

The flux-locked loop (Fig. 7) is based on a direct-coupled readout scheme known as additional

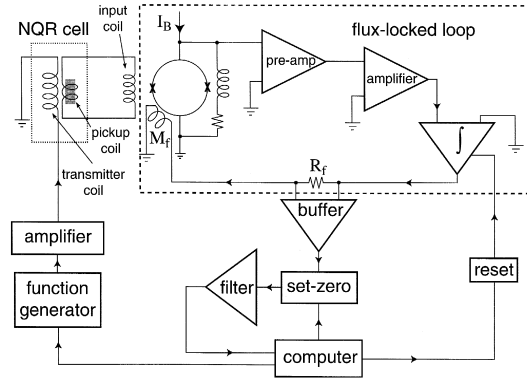

Fig. 7. Block diagram of the pulsed SQUID NQR spectrometer. Dashed lines enclose flux-locked loop while the dotted lines indicate cryogenic components.

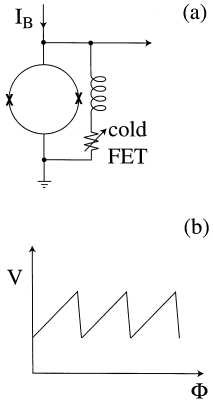

Fig. 8. (a) APF scheme for the dc SQUID, producing the asymmetric voltage vs. flux response shown in (b).

positive feedback (APF) [53–55]; in our system this yields a bandwidth of 0 to 5 MHz [56]. In the APF scheme (Fig. 8a), a coil in series with a variable resistor—actually a cooled MESFET—is connected in parallel with the current-biased SQUID. When a magnetic flux is applied to the SQUID, the resultant change in voltage V causes a current to flow through the coil which in turn induces an additional flux into the SQUID. Depending on the sign of V_Φ, this flux either supports the applied flux, producing positive feedback, or opposes it, producing negative feedback. The resultant $V-\Phi$ curve becomes asymmetric (Fig. 8b), the steeper slope corresponding to positive feedback. One controls the degree of feedback by adjusting the resistance of the MESFET. The enhanced value of V_Φ on the steeper slope, typically 200 $\mu V/\Phi_0$ or more, enables one to connect the SQUID directly to a room temperature preamplifier, which has a typical input voltage noise of 0.5 nV $Hz^{-1/2}$, without sacrificing resolution. After amplification, the signal passes through a single-pole integrator and then, via a feedback resistor R_F, through a coil inductively coupled to the SQUID (Fig. 7). This flux-locked loop maintains the SQUID near the midpoint of the steep part of the $V-\Phi$ curve. The voltage developed across R_F is proportional to the flux in the SQUID. Typically, the flux noise is 2 $\mu\Phi_0$ $Hz^{-1/2}$ and the frequency response (3 dB) is 0–5 MHz.

The sample cells for NMR and NQR are shown in Fig. 9a and b. For NMR, the niobium pickup coil is a Helmholtz pair, each with two turns, while the excitation coil is a second Helmholtz pair, each with 20 turns, orthogonal to the first. Surrounding both coils is a Nb-wire solenoid that we operate in the persistent current mode to supply a static field of up to 15 mT. The entire assembly is surrounded by a Pb shield to exclude external magnetic field fluctuations, and the dewar is surrounded by two concentric shields to attenuate the earth's magnetic field to below 0.1 μT. The sample, typically 0.5 g, is packed into a Pyrex tube that is inserted into the tube supporting the pickup coils. For NQR the cell is similar, except that the pickup coil is a three-turn solenoid surrounded by a larger, 100-turn solenoid that provides the rf excitation (Fig. 9b). In some experiments we use 2 two-turn pickup coils, 15 mm apart and wound in opposition. This gradiometric configuration reduces the signal coupled into the flux

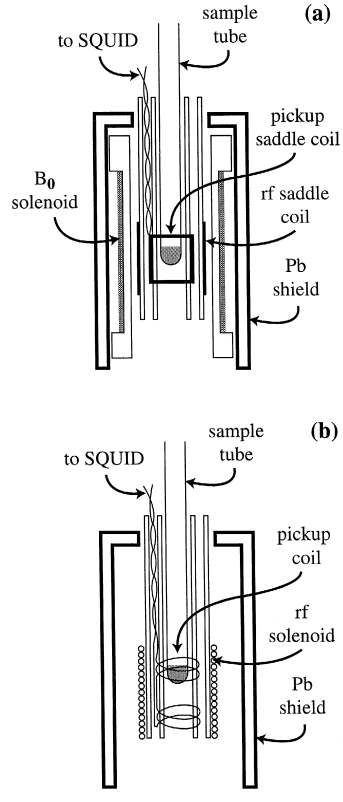

Fig. 9. (a) NMR and (b) NQR cells used in the pulsed SQUID spectrometer.

transformer during the rf excitation. The relative positions of the pickup and excitation coils can be adjusted to give a balance of about 0.5% in the gradiometer.

Finally, we briefly describe the operation of the spectrometer. Triggered by the computer, a function generator (HP 3314A) produces a sinusoidal signal containing between 1 and 30 cycles, starting at zero phase. The pulse is amplified and coupled to the transmitter coil via a low pass filter and four stages of crossed diodes. These diodes present a high impedance to the transmitter coil when the pulse is turned off, thus minimizing the noise coupled into the SQUID during the measurement. The precessing spins induce a flux in the pickup coil which is amplified by the SQUID. Although the problem is less serious for the NQR gradiometer configuration, the rf pulse coupled into the SQUID tends to drive the integrator into saturation, from which it takes a long time to recover after the pulse is turned off. We overcome this problem by shorting the integrator capacitor with a photo-coupled analog switch during the pulse, and opening this switch after the pulse is removed. After the operation of the flux-locked loop has been restored, the output in general contains an offset which is removed by a set-zero circuit. The dead time after the removal of the 1 mT peak-to-peak rf pulse is about 60 μs at 50 kHz and less than 10 μs at 500 kHz and higher. At the end of this dead time, the flux-locked loop is enabled and the FID flux signal is coupled into the SQUID via the flux transformer. We acquire the data using a Techmag pulse programmer for frequencies below 200 kHz, and a digital oscilloscope for higher frequencies; the data are subsequently transferred to a computer.

4.3. Ammonium perchlorate

As a test sample we chose ^{14}N NQR in powdered ammonium perchlorate, NH_4ClO_4, [25] in which the longitudinal relaxation time T_1 is anomalously short even at low temperatures because of its unusually low barrier for four-fold reorientation. At the same time, the transverse relaxation time T_2 is reasonably long, enabling us to obtain sharp spectra. There has been substantial research in other laboratories to understand the structure and the four-fold tunneling dynamics [57]. Neutron diffraction measurements at temperatures between 10 K and 298 K indicate that NH_4ClO_4 has an orthorhombic crystal structure with space group P_{nma}. This structure implies that nitrogen and chlorine atoms lie on planes with mirror symmetry within the unit cell. The four-fold tunneling in this system removes the degeneracy of the vibrational ground state. Using group theory [58] one can characterize the spatial and spin wave functions of each level by one of three irreducible representations of the tetrahedral group T_d, namely A, E, or T. To determine these state labels in zero magnetic field one couples the four $I = 1/2$ protons into three spin manifolds of $S = 2$, 1, and 0. The symmetry of these manifolds within T_d is A, T, and E, respectively. Using this mathematical formalism one can show that T_1 is anomalously short [59].

The sample consisted of 0.5 g of powdered reagent grade ammonium perchlorate packed into an 8 mm diameter NMR tube. The free induction decay shown in Fig. 10a is the result of a two-pulse echo sequence on ^{14}N [25]. The pulses, separated by 5 ms, has

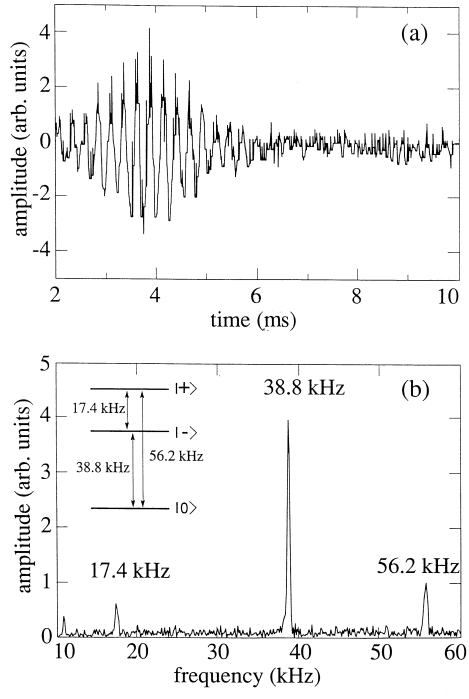

Fig. 10. (a) ^{14}N signal for NH_4ClO_4 following a two-pulse echo experiment at $T = 1.5$ K. (b) Fourier transform of the spin echo. The three peaks at 17.4 kHz, 38.8 kHz, and 56.2 kHz correspond to the transitions shown in the inset.

amplitudes of 3.8 mT and 6.5 mT, respectively, and consisted of a single 45 kHz cycle. Data accumulation began immediately after the second pulse. The signal shown in Fig. 10a is the result of demodulation at 35 kHz, averaged over 16,000 accumulations, obtained with a recycle delay of 300 ms. Fig. 10b shows the Fourier transform of an echo obtained with the same pulse parameters as in Fig. 10a, with the delay time reduced to 4 ms. The spectrum consists of three NQR resonances, 17.4, 38.8, and 56.2 kHz; the two lower resonance frequencies sum to the highest, as one expects for $I = 1$. The small peak at 10.6 kHz arises from magnetoacoustic resonances picked up by the SQUID. These data yield a ^{14}N quadrupole coupling constant $e^2qQ/\hbar = 63.3$ kHz and an asymmetry parameter $\eta = 0.550$. Since there is a possibility of having resonances from the $S = 1$ ^1H manifold, the same two-pulse experiment was performed on ^{15}N ($I = 1/2$) enriched NH_4ClO_4. No three-line NQR signals were found, suggesting that the three-line spectrum in Fig. 10b was indeed due to ^{14}N. The values for the coupling constant and asymmetry parameter are larger by 18% and a factor of 4.3, respectively, than those obtained from high field ^{14}N NMR spectroscopy at room temperature [60].

A further advantage of the pulse technique is the use of the two-pulse echo sequence to measure T_2 and the three-pulse stimulated echo experiment to measure T_1. Fig. 11 shows the decay of the echo

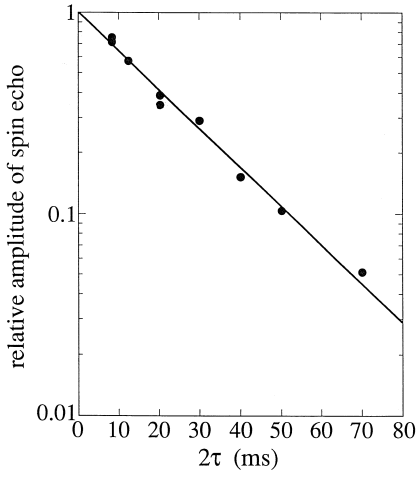

Fig. 11. T_2 relaxation for the $\nu_0 = 38.8$ kHz ^{14}N transition in NH_4ClO_4. The solid circles are experimental data, while the line shows the best fit to an exponential decay with $T_2 = 22$ ms.

maximum as a function of pulse spacing in the same NH_4ClO_4 sample used above. The decay constant, $T_2 = 22 \pm 2$ ms, is a reflection of the homogeneous broadening in the ν_0 ^{14}N transition. Similar data for the stimulated echo sequence yielded $T_1 = 63 \pm 6$ ms. There are two possible mechanisms responsible for the relaxation times in NH_4ClO_4. Since the ^{14}N relaxation times in ND_4ClO_4 were the same to within the errors of those quoted above, the ^1H–^{14}N dipolar coupling makes a negligible contribution to the relaxation rates. This strongly suggests that the dominant relaxation mechanism at 1.5 K is fluctuating electric field gradients, that is, ^{14}N quadrupole coupling.

4.4. Two-dimensional NQR: ruby

An obvious next step in demonstrating the power of the pulsed SQUID spectrometer is the extension of the experiment to more than one dimension. Unfortunately ^{14}N in NH_4ClO_4 is not a good candidate for this study because the signal is small, requiring rather long acquisition times even for one-dimensional NQR. A better choice is ruby, that is Cr^{3+} doped Al_2O_3; the undoped analogue has been well characterized by the cw SQUID technique (Section 3.3). The paramagnetic defect site introduced by Cr^{3+} provides a relaxation pathway for the ^{27}Al [61], permitting rapid signal averaging, typically 30 ms/pulse. The combination of fast relaxation with large signals in the ^{27}Al spectrum of ruby has made it the sample of choice for straightforward calibration of the spectrometer.

The ruby sample contained 300 mm^3 of 0.5 mm diameter spheres doped with 7% of Cr^{3+}. The structure of the unit cell is identical to sapphire (Section 3.3). Fig. 12a and c show the free induction decays for the two NQR lines, averaged over 4000 scans with a 3 Hz repetition rate. The corresponding Fourier transforms are shown in Fig. 12b and d. Digitization of the transients was initiated 10 μs after the pulse was switched off. The two transition frequencies shown in Fig. 12, $\nu_1 = 359$ kHz for $|\pm 1/2> \leftrightarrow |\pm 3/2>$ and $\nu_2 = 714$ kHz for $|\pm 3/2> \leftrightarrow |\pm 5/2>$, agree well with the cw measurements in sapphire reported in Section 3.3. We note that T_1 is less than 30 ms, since we are able to use repetition rates as high as 30 Hz without a noticeable change in signal amplitude.

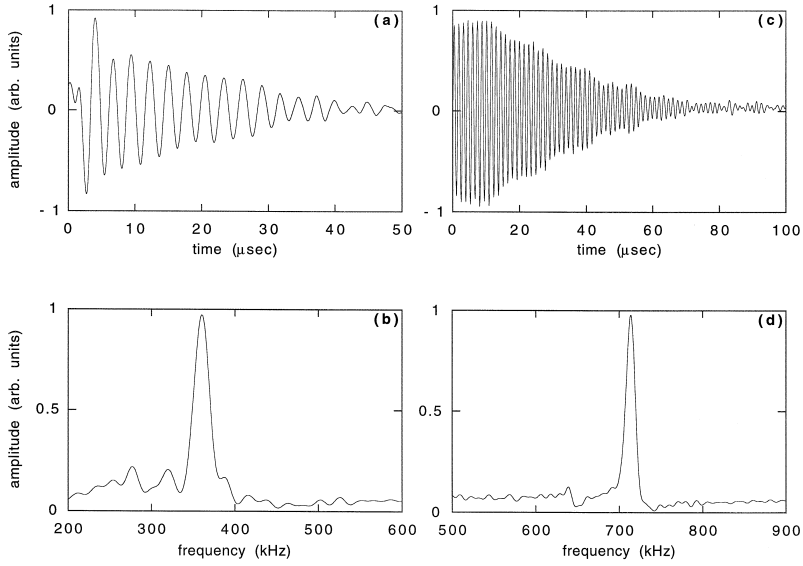

Fig. 12. ^{27}Al NQR data for ruby, $Al_2O_3[Cr^{+13}]$, obtained with a selective pulse. (a) Free induction decay of the 359 kHz transition and (b) its Fourier transform. (c) Free induction decay of the 714 kHz transition, and (d) its Fourier transform.

Although the pulse fields produced by this probe can be substantial (Section 4.2), they were not sufficient to excite both NQR lines with a single frequency. For this reason we introduced a second function generator so that we could simultaneously excite the 359 kHz and 714 kHz resonances. We gated the two synthesizers simultaneously by splitting a single TTL trigger line. The spectrum obtained for the two-frequency pulse is shown in Fig. 13.

It is straightforward to construct a two dimensional data set from this experiment by applying a second, two-frequency pulse a time t_1 after the first pulse. Digitization for a time t_2 yields free induction decays with amplitudes oscillating as a function of t_1 at both 359 kHz and 714 kHz. In the absence of the second, two-frequency pulse, the 359 kHz line oscillates at its own frequency as a function of t_1. The same is true for the 714 kHz transition. Two-dimensional Fourier transformation of a data set obtained without the second pulse produces two peaks only, correlating each of the frequencies υ_1 and υ_2 with itself. In the experiment presented here, the second two-frequency pulse has the net effect of mixing the populations of the two transitions at a time t_1 after the first pulse. In essence the 359 kHz coherence as a function of t_1 is changed into a detectable 714 kHz coherence. This leads to two extra cross peaks in the two dimensional Fourier transform correlating the 359 kHz and 714 kHz lines in ^{27}Al.

The results are shown in Fig. 14. Accurate predictions of the cross-peak amplitude seen in the experiment are not yet available, as detailed calculations including the effects of the pulse intensity and orientation with respect to the ^{27}Al principal axis, as well as the relaxation during t_1, are still in progress. [1]

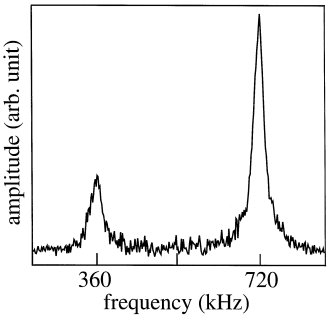

Fig. 13. Fourier transform of the ^{27}Al NQR free induction decay with both transitions irradiated.

[1] Dinh M. TonThat, M. Tomaselli, M.P. Augustine, J. Clarke, unpublished results.

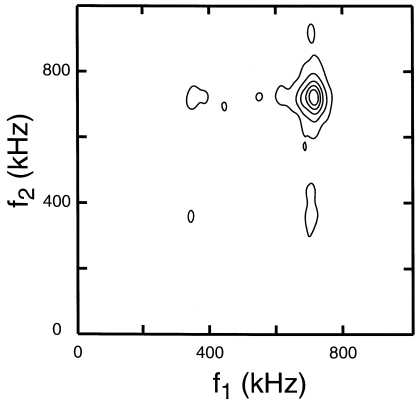

Fig. 14. Two-dimensional NQR spectrum of ^{27}Al in ruby. The spectrum was constructed from 60 free induction decays measured as a function of the interval between the two-frequency pulses. The time between the pulses was incremented in 0.5 μs steps.

This analysis will determine whether the asymmetry in cross-peak amplitude (Fig. 14) is due to different values of T_2 for υ_1 and υ_2 or is the result of inefficient level mixing by the second, two-frequency rf pulse.

This qualitative experiment is the first demonstration of two-dimensional NQR using a SQUID detector. It is hoped that the development of this technique will lead to new insights into ^{14}N NQR spectra in biological systems. Work is currently in progress towards combining these two-dimensional methods with dynamic nuclear polarization to make pulsed ^{14}N NQR a viable option in the study of biological samples.

4.5. Noble gases

The T_1 of ^{129}Xe, polarized by contact with optically pumped Rb, has been measured at magnetic fields down to 5 mT [62]. Lower field measurements were not possible in that study, presumably because the Faraday-induction method was too insensitive to measure such low frequency signals. However, the pulsed SQUID spectrometer has both the bandwidth and sensitivity to measure T_1 at substantially lower magnetic fields, down to 0.09 mT [63].

The optical pumping characteristics for ^{129}Xe are well documented [64], and in our laboratory rely on the apparatus shown in Fig. 15. The pumping cell is a glass cylinder with a volume of 10 cm^3 that is connected to a sample tube via a glass transfer line. Stopcocks are included on this assembly for gas handling. The pumping cell contains both Xe gas and Rb metal. A high vapor pressure of Rb is established by raising the temperature of the cell with a warm stream of N_2 gas (70–90°C). Optical pumping is accomplished by illuminating the cell with circularly polarized light from a 0.5 W diode laser at the wavelength of the D_1 line in Rb, 794.74 nm. As is typical in such experiments, a magnetic field of about 3 mT is applied to split the Rb and Xe levels during the optical pumping. After about 1 h of optical pumping, the cell is cooled to below 40°C to lower the Rb vapor pressure, and the xenon gas is drawn into the sample tube by cooling it in liquid N_2. Here, the Xe freezes in a magnetic field of 0.1 T. The sample tube is inserted into the SQUID spectrometer in the presence of a static magnetic field. A solenoid around the top of the cryostat maintains the Xe in a field of 10 mT during the transfer process, except for a few seconds while the tube is lowered into the coils. Both isotopically enriched xenon (80% ^{129}Xe, 2% ^{131}Xe, EG&G Mound) and natural abundance xenon gas (26.4% ^{129}Xe, 21.2% ^{131}Xe) were used in these experiments. From separate, high-field measurements in our laboratory we estimate the enhanced polarization of the ^{129}Xe to be about 10%.

Fig. 16 shows six ^{129}Xe NMR spectra obtained at fields ranging from 8.9 mT to 0.019 mT, with corresponding Larmor frequencies ranging from 110 kHz to 200 Hz. These spectra were acquired after a single pulse having a tipping angle of 8° for Fig. 16a, and

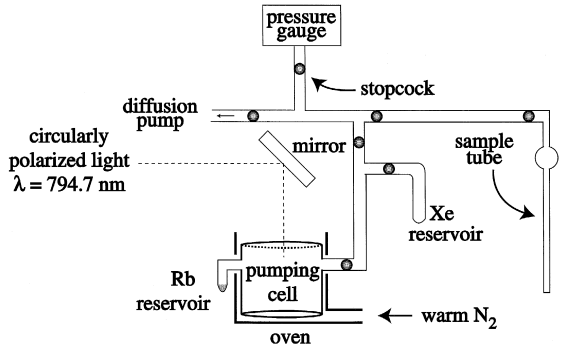

Fig. 15. Optical pumping apparatus, consisting of a 10 cm^3 glass cell, a rubidium reservoir, a xenon reservoir, and a sample cell linked by glass vacuum lines.

nearly 90° for Fig. 16b. Fig. 16b shows the difference observed between ^{129}Xe NMR in isotopically enriched and natural abundance samples. As the magnetic field is reduced to near zero, the full-width at half-maximum approaches 520 ± 60 Hz for the isotopically enriched samples and 340 ± 20 Hz for the natural abundance sample. The line width of these two resonances arises from dipolar broadening due to both ^{129}Xe and ^{131}Xe. No signal could be measured below 0.019 mT as these dipolar fields exceeded the applied magnetic field.

The low field ^{129}Xe T_1 was measured by following the decay of z magnetization with a train of small tipping angle pulses (5–10°). In most cases, this decay was multi-exponential indicating inhomogeneity in the relaxation process. Fig. 17 shows T_1 vs. magnetic field for the enriched sample at 4.2 K, together with the data of Gatzke et al. [62] for fields ranging from 5 to 100 mT. We note that the value of T_1 obtained at the highest field in the current work is a factor of 2 or 3 lower than in the earlier work; we return to this point later. Despite this discrepancy, these more recent, SQUID-based measurements show that T_1 is strongly dependent on magnetic field above a few mT and relatively insensitive below 2 mT; as the magnetic field approaches zero, T_1 saturates at approximately 2000 s.

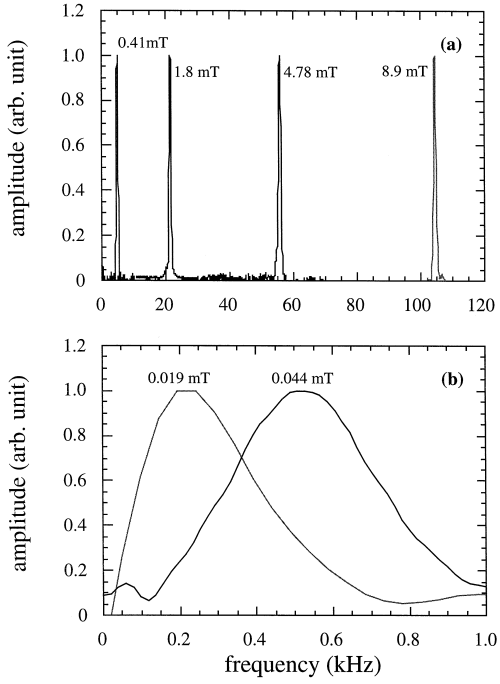

Fig. 16. SQUID-detected ^{129}Xe NMR spectra. (a) Isotopically enriched ^{129}Xe at four different magnetic fields. (b) Isotopically enriched sample at 0.044 mT and natural abundance sample at 0.019 mT.

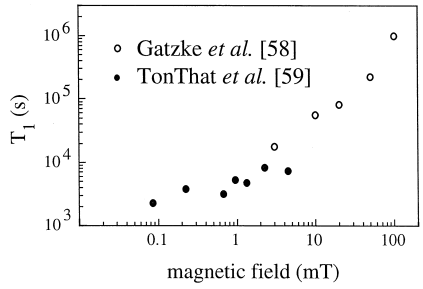

Fig. 17. T_1 for isotopically enriched (solid circles) ^{129}Xe ice as a function of magnetic field. Data of Gatzke et al. [62] are shown as open circles.

It is believed that this spin-lattice relaxation is mostly governed by the ^{129}Xe cross-relaxation to ^{131}Xe, which is then coupled to the lattice by quadrupolar interactions. The fact that the measured T_1 for the ^{129}Xe nuclei is almost independent of magnetic field below 2 mT indicates that the ^{131}Xe line width is very broad, about 20 kHz. Attempts to measure an optically pumped ^{131}Xe NMR signal met with no success suggesting that T_1 is very short for ^{131}Xe. Measurements at 860 mT and at the same temperature [65] yielded a ^{131}Xe line width of 2.4 ± 0.2 kHz, a value still too low to account for the saturation of T_1 in our experiment. A possible explanation of this discrepancy is as follows. In the direct detection of NMR in ^{131}Xe, most of the nuclei contribute to the signal and the line width is dominated by nuclei in the bulk rather than on the surface or at grain boundaries [62]. It is likely that the opposite situation prevails in the observation of the spin-lattice relaxation of ^{129}Xe via cross-relaxation with ^{131}Xe. In that case, the observed magnetic field dependence of T_1 for the ^{129}Xe nuclei suggests that ^{131}Xe near grain boundaries and defects, where higher electric field gradients produce a broader resonance line width, contributes mostly to the cross-relaxation. Since the grain size depends on the details of sample preparation, which is difficult to control, the fact that the relaxation is dominated by nuclear quadrupole

interactions at grain boundaries may well explain why the value of T_1 obtained with the SQUID-spectrometer at about 4.5 mT is lower than that of Gatzke et al. [62].

5. Imaging a room temperature sample

In the foregoing experiments the samples were maintained at liquid ^{4}He temperatures. Although these low temperatures enhance the Boltzmann factor by two orders of magnitude over its room temperature value, as we have seen a significant drawback is the fact that the T_1 can become extremely long. To address this issue, Seton et al. [66,67] and Kumar et al. [68,69] have constructed SQUID based NMR spectrometers in which the sample is maintained at room temperature, while the detection coils and SQUID are cooled in liquid ^{4}He. The spectrometer used by Seton et al. [66,67] uses a tuned flux transformer that sacrifices operational bandwidth for high noise attenuation off resonance. Kumar et al. [69] have adopted the approach used in our laboratory; by leaving the flux transformer untuned they achieved a bandwidth of 2 MHz. We briefly describe the latter work which combines relaxation and chemical-shift contrasting to image mineral oil floating on water.

In one set of experiments, Kumar et al. [69] studied approximately 1 cm^3 of either water or mineral oil, and obtained NMR signals ranging in frequency from 50 to 900 kHz. With the sample at room temperature, they achieved an excellent signal-to-noise ratio for protons at 400 kHz (corresponding to a magnetic field of 9.4 mT) with 200 averages. As a further demonstration, Kumar et al. [69] performed a simple imaging experiment on a sample of mineral oil floating on water. A gradient of about 3 mT/m could be applied in addition to the uniform 9.4 mT field. Fig. 18a shows the ^{1}H NMR spectrum obtained with no gradient field after 50 averages. In Fig. 18b, obtained with a 0.33 Hz repetition rate and 200 averages, the gradient leads to two lines, with the water signal at the higher frequency. When the pulse rate was increased to 1 Hz (Fig. 18c), the water ^{1}H NMR signal decreased significantly because the value of T_1 in water (2–3 s) is much longer than that in mineral oil (tens of milliseconds). Further increases in the repetition rate reduced the water NMR signal to below that of the mineral oil. These results represent a one-dimensional, T_1-contrasted image.

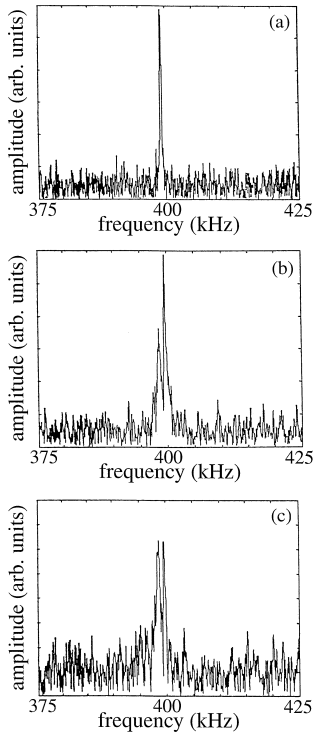

Fig. 18. (From Ref. [69]) (a) ^{1}H NMR signal from water and mineral oil at 9.4 mT and zero gradient. Signal from the same sample with a gradient of 3 mT/m for (b) 0.33 Hz pulse rate and 200 averages, (c) 1 Hz and 200 averages.

6. NMR of small samples

In the experiments described above, the sample volumes have typically been of the order of 1 cm^3. Narasimhan et al. [70] have described a thin-film magnetic susceptometer which has enabled them to detect NMR in a single, 50 μm diameter particle of ^{195}Pt at 4.2 K and 6 mT.

The principle of the susceptometer [71] is illustrated in Fig. 19. The SQUID, fabricated from thin films of niobium, consists of two pickup loops wound in opposite senses and connected in series with the two Josephson junctions. The sample is placed on one of these loops. Each loop of the SQUID is

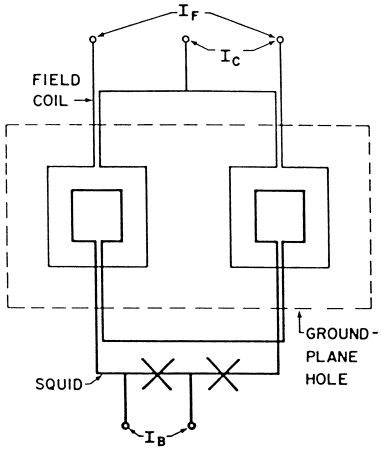

Fig. 19. (From Ref. [71]) Configuration of thin-film miniature susceptometer.

surrounded by a second loop. A current I_F passed through the outer two loops in series ideally couples no net flux to the SQUID; in practice the small imbalance can be compensated by applying a fraction of the current I_C to the center tap. The tipping field is applied to these two loops, while the static field is supplied by a solenoid. In the device used in the NMR experiments, the loops were octagonal and the pickup loops were 50 μm across.

Narasimhan et al. [70] obtained a clearly defined peak from a ^{195}Pt particle at 51 kHz, corresponding to a field of 5.7 mT, averaging over 10^6 pulses. This result is equivalent to the detection of the signal from 2.5×10^{14} nuclei located at the center of the pickup loop. This approach is clearly attractive for the study of NMR in samples containing small numbers of nuclei, and can be extended to fields of up to about 10 mT. An intriguing possibility is to combine this technique with 'scanning SQUIDs' in which the sample at 4.2 K [72], 77 K [73], or room temperature [74] is rastered over the SQUID to obtain a two-dimensional magnetic image.

7. Concluding remarks

The ability of the flux locked SQUID to measure magnetic flux at arbitrarily low frequencies has been exploited in both cw and pulsed NMR and NQR spectroscopy. Of the two, the pulsed technique in principle has much more potential in that it enables one to take advantage of standard spin echo and two-dimensional techniques to obtain relaxation times and spectral simplification. We have seen that it is possible to track the resonances at frequencies down to 200 Hz with a signal-to-noise ratio that is unprecedented. In the current spectrometer in our laboratory the pulsed method is limited in applicability because many materials have extraordinarily long relaxation times at liquid ^{4}He temperatures. In such cases, the pulse cycle rate becomes so slow that signal averaging becomes prohibitively long. Thus, either one must find a way to shorten T_1 or use the cw spectrometer. There are at least two ways of reducing T_1. The first, as implemented by Seton et al. [67] and Kumar et al. [69], is to maintain the sample at room temperature where the values of T_1 for virtually all materials are very much less than at liquid ^{4}He temperatures. This advantage, however, is mitigated by the two-order-of-magnitude reduction in the Boltzmann factor, for which one can compensate by averaging over four-orders of magnitude more pulses. An alternative approach is to maintain the temperature at 4.2 K and to attempt to reduce the T_1 by many orders of magnitude by introducing electrons to provide relaxation, for example, by means of paramagnetic impurities. Furthermore, an appropriate paramagnetic defect site would enable one to enhance the signal substantially by dynamic nuclear polarization [75]. In some biological systems of interest, this could be accomplished by incorporating a nitroxide radical with splittings at 60, 90, and 150 MHz in zero field. These resonances would be easier to saturate than, for example, transition metal impurities where the splitting is often in the microwave region. The combined advantages of faster relaxation and enhanced signal amplitude would greatly increase the list of systems that would be accessible at low temperatures. For samples that are available only in relatively small quantities, one could combine these ideas with the use of the thin film susceptometer.

A logical extension of this work would be to investigate complex molecules with many active nuclei. Such studies are likely to be successful only if one can resort to the multi-dimensional techniques of the NMR spectroscopist. To this end we have made a preliminary observation of a two-dimensional spec-

trum in ruby. If one could successfully combine techniques to increase the T_1 relaxation rate, enhance the signal through dynamic nuclear polarization, and perform multi-dimensional spectroscopy, low frequency, SQUID-based NMR and NQR would become powerful techniques in the elucidation of chemical structure.

In conclusion, it is apparent that SQUID-based spectrometers offer a new window on low-frequency NMR and NQR. Why, then, are these methods not more widely pursued? The reason would seem to be largely that the few spectrometers in existence have been built in the course of graduate research, and their use is consequently restricted to the laboratories in which they were made. Only when professionally engineered 'user-friendly' systems are made commercially available will they become more widely used by the magnetic resonance community.

Acknowledgements

This work was supported by the Director, Office of Energy Research, Office of Basic Energy Sciences, Materials Sciences Division of the U.S. Department of Energy under Grant No. DE-AC03-76SF00098. MPA thanks the National Science Foundation Postdoctoral Fellowship program for support under Grant No. CHE-9504655. The authors thank Marco Tomaselli and Marcia Ziegeweid for helpful suggestions during the course of writing this review, and are indebted to Jeff Reimer for a critical reading of the manuscript.

References

[1] M. Mehring, Principles of High Resolution NMR in Solids, 2nd edn., Springer-Verlag, Berlin, 1983.
[2] C.P. Slichter, Principles of Magnetic Resonance, Springer-Verlag, 3rd edn., Berlin, 1983.
[3] A. Pines, in: W.A. Little (Ed.), Proceedings of the Bloch Symposium, World Scientific, Singapore, 1990, p. 1241.
[4] T.P. Das, E.L. Hahn, in: F. Seitz, D. Turnbull (Eds.), Solid State Physics, Suppl. 1, Academic Press, New York, 1958.
[5] N.F. Ramsey, R.V. Pound, Phys. Rev. 81 (1951) 278.
[6] A.G. Redfield, Phys. Rev. 130 (1963) 589.
[7] N.F. Strombotne, E.L. Hahn, Phys. Rev. 133 (1964) A1616.
[8] D.P. Weitekamp, A. Bielecki, D. Zax, K. Zilm, A. Pines, Phys. Rev. 50 (1983) 1807.
[9] D.T. Edmonds, Phys. Rep. 29 (1977) 233.
[10] F. Noack, Progr. NMR Spectrosc. 18 (1986) 171.
[11] R. Tycko, Phys. Rev. Lett. 60 (1988) 2734.
[12] F.N.H. Robinson, J. Phys. E: Sci. Instrum. 15 (1982) 814.
[13] D. Lee, S.J. Gravina, P.J. Bray, Z. Naturforsch. 45A (1990) 268.
[14] J. Clarke, in: H. Weinstock, R. Ralston (Eds.), SQUIDS: Theory and Practice, The New Superconducting Electronics, Kluwer Academic, Dordrecht, 1993, p. 123.
[15] E.C. Hirschkoff, O.G. Symko, L.L. Vant-Hull, J.C. Wheatly, J. Low Temp. Phys. 2 (1970) 653.
[16] J.H. Bishop, E.C. Hirschkoff, J.C. Wheatly, J. Low Temp. Phys. 5 (1971) 607.
[17] E.P. Day, Phys. Rev. Lett. 29 (1972) 540.
[18] D.J. Meredith, G.R. Pickett, O.G. Symko, J. Low Temp. Phys. 13 (1973) 607.
[19] A.H. Silver, J.E. Zimmerman, Appl. Phys. Lett. 10 (1967) 142.
[20] R.A. Webb, Rev. Sci. Instrum. 48 (1977) 1585.
[21] R.V. Chamberlain, L.A. Moberly, O.G. Symko, J. Low Temp. Phys. 35 (1979) 337.
[22] H. Suzuki, Y. Higashino, T. Ohtsuka, J. Low Temp. Phys. 41 (1980) 449.
[23] K.S. Pickens, D.I. Bolef, M.R. Holland, R.K. Sundfors, Phys. Rev. B 30 (1984) 3644.
[24] U. Werner-Zwanziger, in: D.M. Grant, R.K. Harris, SQUIDs, The Encyclopedia of Nuclear Magnetic Resonance, Wiley, New York, 1995, p. 4559.
[25] N.Q. Fan, J. Clarke, Rev. Sci. Instrum. 62 (1991) 1453.
[26] M.D. Hürlimann, C.H. Pennington, N.Q. Fan, J. Clarke, A. Pines, E.L. Hahn, Phys. Rev. Lett. 69 (1992) 684.
[27] N.Q. Fan, PhD Thesis, University of California, Berkeley, CA.
[28] S.L. Thomasson, C.M. Gould, IEEE Trans. Appl. Supercond. 5 (1995) 3222.
[29] R.C. Jaklevic, J. Lambe, A.H. Silver, J.E. Mercereau, Phys. Rev. Lett. 12 (1964) 159.
[30] F. London, Superfluids, Vol. 1, Wiley, New York, 1950.
[31] B.D. Josephson, Phys. Lett. 1 (1962) 251.
[32] B.D. Josephson, Adv. Phys. 14 (1965) 419.
[33] C.D. Tesche, J. Clarke, J. Low. Temp. Phys. 27 (1977) 301.
[34] M.B. Ketchen, J.M. Jaycox, Appl. Phys. Lett. 40 (1982) 736.
[35] C. Connor, J. Chang, A. Pines, Rev. Sci. Instrum. 61 (1990) 1059.
[36] M. Ziegeweid, PhD Thesis, University of California, Berkeley, CA.
[37] Biomagnetic Technologies, 9727 Pacific Heights Blvd., San Diego, CA 92121-3719.
[38] C. Connor, J. Chang, A. Pines, J. Chem. Phys. 93 (1990) 7639.
[39] C.H. Townes, B.P. Dailey, J. Chem. Phys. 17 (1949) 782.
[40] N. Ishizawa, T. Miyatat, I. Minato, F. Marumo, S. Iwai, Acta Cryst. B 36 (1980) 228.
[41] R.V. Pound, Phys. Rev. 79 (1950) 685.
[42] D.B. Williams, C.B. Carter, Transmission Electron Microscopy: A Textbook for Materials Science, Plenum, New York, 1996.

[43] R.S. Pease, Acta Cryst. 5 (1952) 356.
[44] A.H. Silver, P.J. Bray, J. Chem. Phys. 32 (1960) 288.
[45] J. Thomas Jr., N.E. Weston, T.E. O'Connor, J. Am. Chem. Soc. 84 (1963) 4619.
[46] N.G. Chopra, R.J. Luyken, K. Cherrey, V.H. Crespi, M.L. Cohen, S.C. Louie, A. Zettl, Science 259 (1995) 966.
[47] R. Tycko, S.J. Opella, J. Am. Chem. Soc. 108 (1986) 3531.
[48] D.T. Edmonds, P.A. Speight, Phys. Lett. 34A (1971) 325.
[49] E.R. Slusher, E.L. Hahn, Phys. Rev. 166 (1968) 332.
[50] U. Werner, B. Black, M. Ziegeweid, A. Pines, Chem. Phys. Lett. 209 (1993) 17.
[51] D.T. Edmonds, Phys. Rep. 29 (1977) 233.
[52] J.P. Yesinowski, M.L. Buess, A.N. Garroway, M. Ziegeweid, A. Pines, Anal. Chem. 67 (1995) 2256.
[53] D. Drung, R. Cantor, M. Peters, H.J. Scheer, H. Koch, Appl. Phys. Lett. 57 (1990) 406.
[54] D. Drung, R. Cantor, M. Peters, T. Ryhanen, H. Koch, IEEE Trans. Magn. MAG-27 (1991) 3001.
[55] D. Drung, H. Matz, H. Koch, Rev. Sci. Instrum. 66 (1995) 3008.
[56] D.M. TonThat, J. Clarke, Rev. Sci. Instrum. 67 (1996) 2890.
[57] C.S. Choi, H.J. Prask, E. Prince, J. Chem. Phys. 61 (1974) 3523.
[58] S. Greiger, H. Friedrich, B. Asmussen, K. Guckelsberger, D. Nettling, W. Press, R. Scherm, Z. Phys. B 87 (1992) 203.
[59] A. Birczyn'ski, Z.T. Lalowicz, Z. Olejniczak, M. Punkkinen, Solid State NMR 7 (1996) 105.
[60] J. Bastow, S.N. Stuart, J. Phys. Condens. Matter 1 (1989) 4649.
[61] J. Winter, C.R. Acad. Sci. 249 (1959) 2192.
[62] M. Gatzke, G.D. Cates, B. Driehuys, D. Fox, W. Happer, B. Saam, Phys. Rev. Lett. 70 (1993) 690.
[63] Dinh M. Ton That, M. Ziegeweid, Y.-Q. Song, E.J. Munson, S. Appelt, A. Pines, John Clarke, Chem. Phys. Lett., submitted.
[64] M.P. Augustine, K.W. Zilm, J. Chem. Phys. 105 (1996) 2998.
[65] W.W. Warren Jr., R.E. Norberg, Phys. Rev. 154 (1967) 277.
[66] H.C. Seton, D.M. Bussell, J.M.S. Hutchinson, I. Nicholson, D.J. Lurie, Phys. Med. Biol. 37 (1992) 2133.
[67] H.C. Seton, D.M. Bussell, J.M.S. Hutchinson, D.J. Lurie, IEEE Trans. Magn. 5 (1995) 3218.
[68] S. Kumar, B.D. Thorson, W.F. Avrin, J. Magn. Reson. Ser. B 107 (1995) 252.
[69] S. Kumar, W.F. Avrin, B.R. Whitecotton, IEEE Trans. Magn. 32 (1996) 5261.
[70] L.R. Narasimhan, M. Takigawa, M.B. Ketchen, Appl. Phys. Lett. 65 (1994) 1305.
[71] M.B. Ketchen, T. Kopley, H. Ling, Appl. Phys. Lett. 44 (1984) 1008.
[72] J.R. Kirtley, M.B. Ketchen, K.G. Stawiasz, W.J. Gallagher, S.H. Blanton, S.J. Wind, Appl. Phys. Lett. 66 (1995) 1138.
[73] R.C. Black, A. Mathai, F.C. Wellstood, E. Dantsker, A.H. Mikilich, D.T. Nemeth, J.J. Kingston, J. Clarke, Appl. Phys. Lett. 62 (1993) 2128.
[74] T.S. Lee, E. Dantsker, J. Clarke, Rev. Sci. Instrum. 67 (1996) 4208.
[75] A. Abragam, Principles of Nuclear Magnetism, Oxford Univ. Press, New York, 1989, p. 354.